

# Data-Efficient Classification of Radio Galaxies

Ashwin Samudre<sup>1</sup>★, Lijo T. George<sup>2</sup>, Mahak Bansal<sup>3</sup>, Yogesh Wadadekar<sup>2</sup>

<sup>1</sup>European Molecular Biology Laboratory, Heidelberg, Germany

<sup>2</sup>National Centre for Radio Astrophysics, TIFR, Post Bag 3, Ganeshkhind, Pune 411007, India

<sup>3</sup>Viterbi School of Engineering, University of Southern California, CA, USA

Last updated xxx; in original form yyy

## ABSTRACT

The continuum emission from radio galaxies can be generally classified into different classes like FRI, FRII, Bent, or Compact. In this paper, we explore the task of radio galaxy classification based on morphology using deep learning methods with a focus on using a small scale dataset ( $\sim 2000$  samples). We apply few-shot learning techniques based on Siamese Networks and transfer learning techniques using a pre-trained DenseNet model with advanced techniques like cyclical learning rate, discriminative learning to train the model rapidly. We achieve a classification accuracy of over 92% using our best performing model with the biggest source of confusion being between Bent and FRII type galaxies. Our results show that focusing on a small but curated dataset along with the use of best practices to train the neural network can lead to good results. Automated classification techniques will be crucial for upcoming surveys with next generation radio telescopes which are expected to detect thousands of new radio galaxies in the future.

**Key words:** galaxies: active – techniques: image processing

## 1 INTRODUCTION

The radio continuum sky contains a wide variety of sources. Some are compact sources while others are extended. Compact sources are unresolved sources with a single source component whereas extended sources are any whose sizes are greater than the effective resolution of the telescope.

In some galaxies, emission from the central Active Galactic Nucleus (AGN) is seen in the form of relativistic jets which manifest as radio synchrotron emission. These radio jets usually come in pairs and extend outwards in diametrically opposite directions. When they collide with the denser parts of the intergalactic medium, they give rise to the radio lobes. The morphology of the twin jets and radio lobes is used to broadly classify radio galaxies into FRI and FRII types (Fanaroff & Riley 1974). In FRI galaxies, the peak of the emission is closer to the central core and the emission brightness decreases farther away from the centre. On the other hand, the radio emission in FRII galaxies increases in brightness outwards culminating in bright hotspots at the outer edge of the jet emission. See Figure 1 for typical examples of FRI and FRII galaxies drawn from our sample.

Apart from these two broad classes, some radio galaxies also show a more complex morphology. If the angle between the jets in the radio galaxy is significantly less than  $180^\circ$ , then it can be classified as a Bent-Tail (BT) galaxy. BT galaxies can be further sub-classified as Narrow-Angle Tail (NAT) or Wide Angle Tail (WAT)

galaxies based on the angle between the two jets (Rudnick & Owen 1976). In NATs, the jets are so bent that the entire radio structure lies on one side of the optical galaxy (Miley et al. 1972) whereas in WATs the angle of projection between the jets is  $\sim 60^\circ$  (Dehghan et al. 2014). Bent Tail galaxies are believed to form in dense environments such as galaxy clusters. The bent tail phenomenon is usually attributed to the large ram-pressure exerted on the jets as a result of the motion of the host galaxy through the cluster medium (Miley et al. 1972; Rudnick & Owen 1976; Burns 1990) or due to the turbulent movement of the ICM (Intra-Cluster Medium) during a merger (Burns 1990; Burns et al. 1996; Roettiger et al. 1996). As such, they can be effectively used as tracers for the presence of galaxy clusters, particularly at high redshifts (Blanton et al. 2000, 2003; Mao et al. 2009, 2010; Wing & Blanton 2011; Dehghan et al. 2014). It is expected that the upcoming Evolutionary Map of the Universe (EMU) survey (Norris et al. 2011) will be able to detect many new galaxy clusters via this method.

Traditionally, radio galaxy classification has been carried out by visual inspection of radio continuum images. Large area radio surveys like the NVSS (Condon et al. 1998), FIRST (Becker et al. 1995), SUMSS (Bock et al. 1999) have been used to identify and classify radio galaxies based on their morphology. The Radio Galaxy Zoo (RGZ) project aims to use citizen scientists to assist in the identification and classification of candidate radio galaxies (Banfield et al. 2015). In the future, next generation radio telescopes like MeerKAT (Jonas & MeerKAT Team 2016), ASKAP (Johnston et al. 2008) and eventually the SKA (Carilli et al. 2004) will significantly improve in sensitivity and detect millions of new radio

★ Contact e-mail: ashwin.samudre@embl.de



**Figure 1.** A typical example of an FRI (top) and FR II (bottom) type radio galaxy from our sample.

galaxies. Given these astronomical numbers, manual classification of radio galaxies would be highly impractical, if not impossible. As a result, astronomers need to identify an automated way to precisely classify radio galaxies based on their morphology.

Automated classification algorithms using machine learning and deep learning techniques are extremely useful for this purpose. Machine learning techniques have been widely applied to astronomical problems in recent years. See [Fluke & Jacobs \(2020\)](#) for a recent review.

Classification of optical galaxies using artificial neural networks has been a particularly active field of research ([Philip et al. 2002](#); [Dieleman et al. 2015](#); [Huertas-Company et al. 2015](#); [Ostrovski et al. 2017](#); [Schawinski et al. 2017](#); [Hocking et al. 2018](#); [Martin et al. 2020](#); [Cheng et al. 2020](#)). [Aniyan & Thorat \(2017\)](#) were the first to employ a CNN (Convolutional Neural Network) to classify radio galaxies using FIRST survey images. Since then several other researchers ([Alhassan et al. 2018](#); [Lukic et al. 2018](#); [Ma et al. 2019](#); [Lukic et al. 2019](#); [Wu et al. 2019](#); [Tang et al. 2019](#)) have used different variations of the standard CNN architecture to attempt radio galaxy classification.

Recently, deep learning ([LeCun et al. 2015](#)) algorithms have shown remarkable efficacy in image classification and speech recognition tasks across diverse fields. McCulloch & Pitts introduced the McCulloch-Pitts Neuron ([McCulloch & Pitts 1943](#)) in 1943, which is considered as the initial version of the Artificial Neural Network. Further work by [Hebb \(1949\)](#), [Rosenblatt \(1958\)](#) laid the foundation for modern neural networks. The current deep learning era started with the introduction of Deep Belief Networks by [Hinton et al. \(2006\)](#) (see [Wang et al. \(2017\)](#) for a comprehensive history of deep learning). The term deep learning itself is associated with the collection of new techniques mainly based on Neural Networks. In these networks, inputs are fed into the input layer propagating through one or more hidden layers and finally linking to the output layer. A layer is mainly a set of nodes, sometimes referred to as units, connected to the immediately preceding and following layers. The input layer nodes are associated with the inputs from the dataset of

interest. In deep neural networks, multiple layers are present (hence the term deep) and starting with the second layer, each layer essentially performs the feature construction based on the output of the previous layers which in turn acts as the input to the current layer. The output from the final layer is compared with the expected output and the difference (also called the ‘error’) is propagated backward (called backpropagation ([Rumelhart et al. 1986](#))), through all the layers to adjust the units in each layer and the process is repeated. This backpropagation process helps in better optimisation of the network for each input dataset.

In this work, we have implemented a method to perform automated morphological classification of radio galaxies using deep learning into four important classes - FRI, FR II, Bent, and Compact. The novel feature of this work is the focus on creating a classifier with fewer data samples while still striving for maximum accuracy. [Roh et al. \(2018\)](#) provide an overview of the role of data in machine learning and deep learning techniques. An approximate rule of thumb is that we need at least 1000 samples per class in the task. The State of the Art results for Computer Vision tasks ([Yalniz et al. 2019](#); [Kolesnikov et al. 2019](#)) based on ImageNet ([Deng et al. 2009](#)) and MNIST ([LeCun et al. 2010](#)) datasets have used architectures like ResNet ([He et al. 2016](#)), DenseNet ([Huang et al. 2017](#)) for ideal performance but the sample size for these tasks has been at least 1000 images per class. [Luo et al. \(2018\)](#) discuss the impact of data sample size in image classification tasks and show that sample size affects the performance as we increase the number of classes in the task. For the transfer learning approach on image classification tasks, [Soekhoe et al. \(2016\)](#) discuss that in case of a limited data sample, training only specific layers can provide performance similar to a model trained from scratch with a large dataset.

The previously mentioned approaches to build a classifier for radio galaxies have used a large amount of data (at least 10000 samples in each class) for experiments. Where necessary, sample sizes have been increased with the use of techniques like oversampling and data augmentation ([Krizhevsky et al. 2012](#)). In [Alhassan et al. \(2018\)](#), authors achieved an overall accuracy above 94% (with the same 4 classes as this work - FRI, FR II, Bent, Compact for classification) using more than 21000 samples. [Aniyan & Thorat \(2017\)](#) performed a 3 class (FRI, FR II and Bent) classification using a small original dataset (716 total samples) but above 25000 samples for experiments with substantial use of augmentation. [Ma et al. \(2019\)](#) implemented an unsupervised pre-training technique on the unlabeled samples and later use this pre-trained model to classify the labeled samples as a 6 class classification task. They use 1442 labeled and 14245 unlabeled samples and at least 4900 samples per class in case of experiments with augmentation in their two-step approach. [Lukic et al. \(2018\)](#) performed 4 class (Compact, Single extended, Two-Component extended and Multi-component extended) classification using a total of 141032 samples via augmentation (21933 original samples) for 4 classes. [Wu et al. \(2019\)](#) used object detection and classification techniques while using more than 10000 samples for their experiments. The authors also leverage the transfer learning technique by loading pre-trained model weights based on ImageNet dataset. [Tang et al. \(2019\)](#) implemented transfer learning approach while maintaining the idea of domain transfer. The authors used NVSS ([Condon et al. 1998](#)) and FIRST ([Becker et al. 1995](#)) catalog samples and performed 1) pre-training of the model on NVSS data and transfer the weights for FIRST data and 2) pre-train model on FIRST data, transfer weights for NVSS data. Their task is 2 class (FRI and FR II) i.e. binary classification task. [Lukic et al. \(2019\)](#) performed a 3 class (Unresolved, FRI and FR II) classification using a model pre-trained on ImageNet dataset

and 15936 total image samples. We have limited our data sample size to  $\sim 2000$  images for initial experiments and  $\sim 2700$  images for the experiments with the balanced classes. As we increase the number of data samples, we can capture the distribution of the data in a better way. However, obtaining a large number of samples is not always feasible. Thus, we need to develop algorithms that can perform better even with a limited amount of data. In this work, we apply few-shot learning and transfer learning techniques. Our results show that with the use of a curated dataset and a well designed neural network architecture, higher accuracy can be obtained even with very less amount of data for the classification task.

The paper is organised as follows: Section 2 presents the overall approach towards the problem and includes the data sample construction used for the experiments, the initial approach of few-shot learning technique and its intuition to work efficiently with less amount of data, transfer learning introduction with a description of pre-trained models and the specific architecture used for our experiments. Section 3 presents the experimental details where we try out and apply the optimum parameters to obtain the results. In section 4, we discuss the results, choice of hyperparameters and the scope for further work.

## 2 METHODOLOGY

### 2.1 Data Sample construction

Our radio galaxy sample was compiled using data from several catalogs. We used the catalog by Proctor et al. (2011) for bent-tail galaxies (BENT). For compact sources (Compact) we combined the FR0 catalog by Baldi et al. (2018) and the CoNFIG (Combined NVSS-FIRST Galaxies) sample (Gendre & Wall 2008; Gendre et al. 2010). We only used the sources classified as “Compact (C)” for this sample. The sample of FRI galaxies included the FRICAT by Capetti et al. (2017a) as well as the sources classified as FRI in the CoNFIG sample. Similarly, the FRII sample of galaxies was combined from the FRIICAT by Capetti et al. (2017b) and the sources classified as FRII in the CoNFIG sample. We did not use sources classified as “unresolved” from the CoNFIG catalog.

The complete data sample initially contained 412 Bent, 332 Compact, 321 FRI, and 606 FRII sources. We manually inspected the FIRST image for every galaxy in our sample and discarded a few galaxies based on 1) Presence of multiple sources in a single image, 2) High noise component in the image, 3) Source present but concentrated at the extreme (L/R) of the image. Through this manual procedure, we removed 7 samples from the Bent set, 26 samples from the Compact set, 32 samples from the FRI set, 29 samples from the FRII set. About  $\sim 25\%$  samples from each class were used for validation purposes. The test set images were obtained separately per category. The numbers of objects in each category are listed in Table 1.

Similar to Aniyán & Thorat (2017) some pre-processing was performed on the images before being used. Noise statistics were calculated in every image and all pixels below  $3\sigma$  were clipped.

We handle the class imbalance in accordance with the majority class (FRII) via upsampling the other 3 classes. The upsampling is performed via duplication of randomly selected samples from the original set and combining these with the original set. The numbers of objects in balanced dataset for each category are listed in Table 2.

To work with this amount of data, we initially implemented the Few-Shot learning approach and used Siamese Networks for the classification purpose.

**Table 1.** Final data sample distribution: number of total images, training, validation and testing images (**Original set**).

Type	Number of samples	Train	Validation	Test
Bent	508	305	100	103
Compact	406	226	80	100
FRI	389	215	74	100
FRII	679	434	144	101
Total	1982	1180	398	404

**Table 2.** Final data sample distribution with balanced classes: number of total images, training, validation and testing images.

Type	Number of samples	Train	Validation	Test
Bent	680	433	144	103
Compact	675	431	144	100
FRI	674	430	144	100
FRII	679	434	144	101
Total	2708	1728	576	404

### 2.2 Few-Shot Learning

A variety of algorithms in deep learning have performed efficiently in terms of pattern recognition for image data. These algorithms often need large amounts of data and break down when forced to make predictions about data for which little supervised information is available. The ability to acquire and recognize new patterns is strong in humans. In particular, people seem to be able to understand new concepts quickly and then recognize variations on these concepts in future cases (Lake et al. 2011). The deep learning algorithms are unable to learn the features for a class from a single image and generalize this information for the unseen images from the same class. The few shot learning approach is used to provide the machine with a quick understanding of the different images and their corresponding classes.

The few shot learning techniques are devised to classify the image samples correctly even when the availability of the supervised data is limited. It is a procedure that resembles human-like learning.

#### 2.2.1 Advantages of Few Shot Learning (FSL):

- Few Shot Learning can help in the reduction of the data-gathering efforts as well as the computation time and cost that arises with a large amount of data. The image classification accuracy ( $P$ ) improves with the experience ( $E$ ) obtained by a few labeled images for each class of the target ( $T$ ), and the prior knowledge extracted from other classes, such as raw images to co-training (Blum & Mitchell 1998). Methods succeed in this task usually have higher generality, therefore they can be easily applied for tasks with large training samples.

- Few Shot Learning can help in training suitable models for rare cases when the supervised data are limited. Although this is a common situation in many astronomical problems, to our knowledge, this work represents the first application of few shot learning in astronomy.

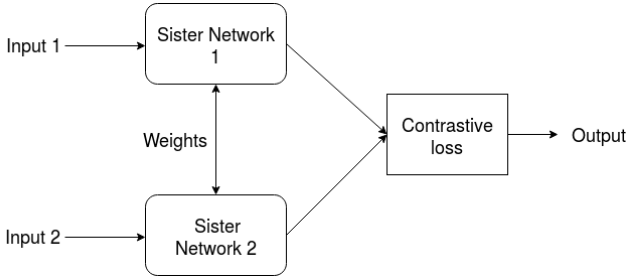


**Figure 2.** Architecture of a simple Siamese Network.

### 2.2.2 Siamese networks

Siamese networks (Koch 2015) are neural networks containing two or more identical subnetwork components. A siamese network can be visualized as shown in Figure 2.

The network is called ‘Siamese’ as the subnetworks have identical architecture and the weights are also shared among them. Siamese network architecture is based on the idea that it can learn useful data descriptors that assist to compare the inputs of the respective subnetworks. The network handles different types of input such as numerical data (in this case the subnetworks are usually formed by fully-connected layers), image data (with Convolutional Neural Networks as subnetworks, current case) or even sequential data such as sentences or time signals (with Recurrent Neural Networks as subnetworks). In training deep neural networks, an activation function is used to define the output of a given node. It helps to avoid the linearity between the outputs of subsequent layers and thus the network can learn the complex patterns from the data.

Batch normalization (Ioffe & Szegedy 2015b) (also referred to as BatchNorm) is another technique to normalize the inputs to each layer during training, which is performed using mean and standard deviation of the values in the current batch. This helps to reduce the difference in input parameters (obtained from a variety of input samples) to each layer. Siamese Networks performs pairwise learning and learns to find the similarity between the pair of images as opposed to a traditional CNN that learns to classify a single image predominantly via loss function like cross-entropy loss.

Although accuracy is often the primary evaluation metric for the performance of classification problems, to quantify the performance of our network’s classification ability, we use other metrics such as Precision, Recall, and F1-score. These metrics provide detailed insights based on the performance of the classifier for each class. The precision  $P$  (purity) and recall  $R$  (completeness) are defined as follows:

$$Precision(P) = \frac{TP}{TP + FP} \quad (1)$$

$$Recall(R) = \frac{TP}{TP + FN} \quad (2)$$

The F1 score is interpreted as the weighted average of precision and recall. The accuracy is the overall accurate prediction by the classifier across all the classes.

$$F1 - score = \frac{2 \times Precision \times Recall}{Precision + Recall} \quad (3)$$

$$Accuracy = \frac{TP + TN}{TP + FP + TN + FN} \quad (4)$$

**Table 3.** Test metrics: Siamese Networks, original dataset

Class	Precision	Recall	F1-Score	Support
Bent	53.41%	45.63%	49.21%	103
Compact	96.77%	90%	93.26%	100
FRI	67.2%	84%	74.67%	100
FRII	69.39%	67.33%	68.34%	101
avg/ total	71.69%	71.74%	71.37%	404

where TP=true positive, TN=true negative, FP=false positive, FN=false negative.

- True Positive (TP) is when the source is predicted as ‘x’ and it is actually ‘x’.
- False Positive (FP) is when the source is predicted as ‘x’ and it is not actually ‘x’.
- True Negative (TN) is when the source is predicted as not ‘x’ and it is actually not ‘x’.
- False Negative (FN) is when the source is predicted as not ‘x’ and it is actually ‘x’.

The precision, recall, F1 score, and accuracy metrics were calculated for both the validation and test data sets to assess the performance in each experiment with the corresponding model. We also provide the confusion matrix, another tool to visualize the performance of the classifier for each experiment. Confusion matrix helps in calculation of the metrics like accuracy, precision, recall and thus F1-score per class.

We perform the experiments in two different settings: original imbalanced dataset and the balanced dataset obtained via upsampling of minority classes with respect to the majority class. Since we will be referring to two set of experiments frequently, we use the following notations. Version 1: original imbalanced dataset experiments, Version 2: balanced dataset experiments.

### 2.2.3 Few-Shot Learning experiments and results

We used the open source PyTorch (Paszke et al. 2019) framework, Python version 3.6.7 for our experiments and Nvidia P100 graphics processing unit (GPU) for the hardware support.

We implemented a customized data loader in PyTorch to feed input pairs to the Siamese Networks. We use the architecture described for Siamese networks which involves five convoluted layers with batch normalization and two fully connected layers with ReLU activation function. The loss function used here is Contrastive Loss Function (Hadsell et al. 2006). In the testing phase, K-nearest neighbors technique is used to classify images. The test image is compared to the embeddings of all the images in training data (stored earlier) and the class of images that are closest to this image (k nearest neighbors) is assigned to the test image.

The performance of Siamese Networks on the original dataset provided an overall accuracy of 71.53%. The performance metrics can be observed in Table 3. The true positive values per class can be observed in the Figure 3.

Further, we tried the same network on balanced dataset. The overall accuracy improved marginally to a value of 74.26%. Performance metrics can be observed in Table 4. The details per class can be observed in Figure 4.

Although the results of Siamese Networks in Few Shot Learning are encouraging, we wanted to see if the use of other more



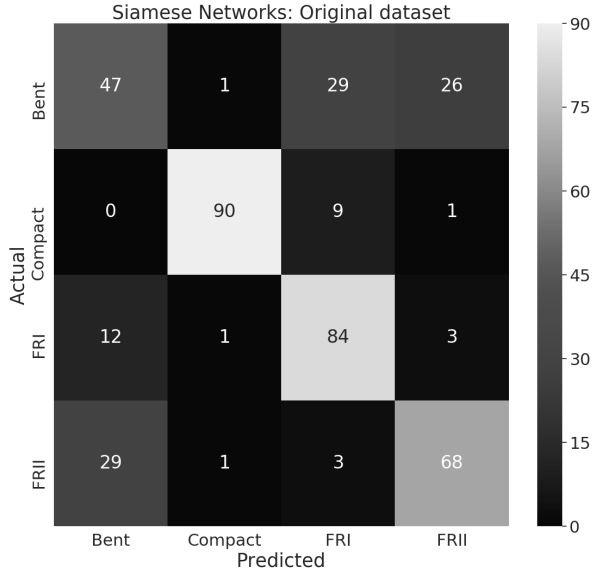


Figure 3. Siamese Networks, Dataset Version 1: test data confusion matrix.

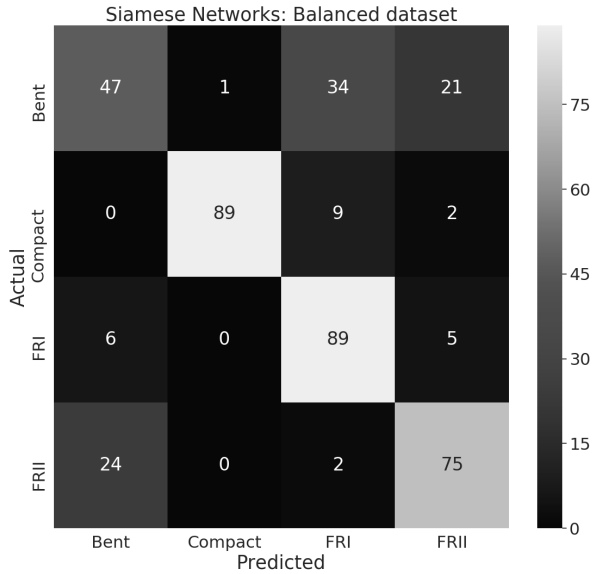


Figure 4. Siamese Networks, Dataset Version 2: test data confusion matrix.

Table 4. Test metrics: Siamese Networks, balanced dataset

Class	Precision	Recall	F1-Score	Support
Bent	61.03%	45.63%	52.22%	103
Compact	98.88%	89%	93.68%	100
FRI	66.41%	89%	76.06%	100
FRII	72.81%	74.26%	73.53%	101
avg/ total	74.78%	74.47%	73.87%	404

sophisticated techniques produces better results. We therefore switched to the Transfer Learning approach using the same input data.

### 2.3 Transfer Learning

Transfer learning (Pratt 1993) is a technique in machine learning which focuses on storing the knowledge gained while solving one problem and applying it to a different but related problem (See Tan et al. (2018) for an overview of deep transfer learning). The definition of transfer learning is given in terms of domain and task. The domain  $D$  consists of: a feature space  $X$  and a marginal probability distribution  $P(X)$ , where  $X = x_1, \dots, x_n$  belong to  $X$ . Given a specific domain,  $D = \{X, P(X)\}$ , a task  $T$  consists of two components: a label space  $Y$  and an objective predictive function  $f$  (denoted by  $T = \{Y, f\}$ ), which is learned from the training data consisting of pairs  $\{x_i, y_i\}$ , where  $x_i$  belongs to  $X$  and  $y_i$  belongs to  $Y$ . The function  $f$  can be used to predict the corresponding label,  $f(x)$ , of a new instance  $x$  (Pan & Yang 2009). In retrospect, transfer learning is the ability to utilize existing knowledge from the source learner in the target task.

#### Pre-trained models

One important requirement for transfer learning is the availability of models that perform well on source tasks. Pre-trained models are trained on a large amount of data with a variety of classes. The weights of such a network are set to obtain the low-level features like shapes, edges identified by the initial layers of the network efficiently. In this work, we use the method of transfer learning by loading weights pre-trained on ImageNet dataset and the architecture used is DenseNet and its variants. We also worked with some other architectures than the final one used here with no improvement in the performance, but we do not claim to have explored the complete parameter set.

We could not get satisfactory results with a custom convolutional neural network architecture and thus opted for DenseNet architecture.

#### 2.3.1 DenseNet Architecture

In Convolutional Neural Networks, the input image goes through multiple convolutions to obtain high-level features. Feature maps are the collective output of the convolution operation applied over the whole input image by all the convolution filters. Skip connections are the connections to the current layer from layers other than the immediately preceding layer. In DenseNet, the feature maps are concatenated from each of the previous layers along with the addition of the skip connections obtained from the previous layers. Thus, each layer receives collective knowledge from all the previous layers. Traditional CNN with ‘L’ layers have ‘L’ connections between the subsequent layers whereas DenseNet has  $L \times (L + 1) / 2$  direct connections. This helps to avoid the learning of redundant feature maps and a reduction in the requirement of total parameters of the network. The important element in DenseNet is the dense block which is composed of the Batch Normalization layer (Ioffe & Szegedy 2015a), ReLU activation function (Nair & Hinton 2010) and  $3 \times 3$  convolution layer and the dimensions of the feature maps remain constant within a block. The dense blocks contain transition layers in between them consisting of Batch Normalization, Convolution, and Pooling layers. Growth rate (K) of the network due to concatenation of the feature maps at each layer ‘L’ can be formulated as  $K(L) = K(0) + K \times (L - 1)$  and it regulates the amount

**Table 5.** DenseNet-161 architecture

# Layer	Function	Input tensor size	Activation	Stride	Output tensor size	No. of parameters	# Block
0	Input	3 x 224 x 224	-	-	-	0	-
1	conv	3 x 224 x 224	ReLU	2	96 x 112 x 112	14112	-
1	pooling	96 x 112 x 112	-	2	96 x 56 x 56	0	-
2-13	[1 x 1 conv, 3 x 3 conv] x 6	96 x 56 x 56	ReLU	2	48 x 56 x 56	82944	1
14	conv	384 x 56 x 56	ReLU	2	192 x 56 x 56	73728	-
14	pooling	192 x 56 x 56	-	2	192 x 28 x 28	0	-
15-38	[1 x 1 conv, 3 x 3 conv] x 12	192 x 28 x 28	ReLU	2	48 x 28 x 28	82944	2
39	conv	768 x 28 x 28	ReLU	2	384 x 28 x 28	294912	-
39	pooling	384 x 28 x 28	-	2	384 x 14 x 14	0	-
40-111	[1 x 1 conv, 3 x 3 conv] x 36	384 x 14 x 14	ReLU	2	48 x 14 x 14	82944	3
112	conv	2112 x 14 x 14	ReLU	2	1056 x 14 x 14	2230272	-
112	pooling	1056 x 14 x 14	-	2	1056 x 7 x 7	0	-
113-160	[1 x 1 conv, 3 x 3 conv] x 24	1056 x 7 x 7	ReLU	2	48 x 7 x 7	82944	4
161	BatchNorm2d	48 x 7 x 7	-	-	2208 x 7 x 7	4416	-
161	avgpool	2208 x 7 x 7	-	2	2208 x 1 x 1	0	-
161	maxpool	2208 x 1 x 1	-	2	2208 x 1 x 1	0	-
161	Flatten	2208 x 1 x 1	-	-	4416	0	-
161	BatchNorm1d	4416	-	-	4416	8832	-
161	Dropout	4416	-	-	4416	0	-
161	Linear	4416	ReLU	-	512	2261504	-
161	BatchNorm1d	512	-	-	512	1024	-
161	Dropout	512	-	-	512	0	-
161	Linear	512	-	-	4	2052	-

of information added to the network at each layer. At the end of the last block, global average pooling is performed and then a softmax activation is attached to get the final result.

The DenseNet architecture has two important advantages:

- (i) The availability of connections between all the layers helps to propagate the error or the gradient more directly. The earlier layers can get feedback from the final layer rapidly.
- (ii) The input received by the current layer has knowledge from all the preceding layers leading to diversified features and richer patterns. This helps to obtain smoother decision boundaries. It also explains why DenseNet performs well when training data are insufficient - the central insight for our experiments.

### 2.3.2 Experimental setup and parameter selection

We used the Fastai (Howard et al. 2018) library, Python version 3.6.7 for our experiments and Nvidia P100 graphics processing unit (GPU) for the hardware support. We set the batch size of 32 and the image size of  $224 \times 224$ , the data samples are normalised using the ImageNet stats. We use the learning rate finder method based on the cyclical learning rates (Smith 2015) to obtain the optimal learning rate. This method performs a mock training run starting with a smaller value for the learning rate which is modified after each batch. It searches the maximum learning rate at which there is still some improvement in terms of a decrease in the error. The learning rate either increases or decreases based on the outcome from the latest batch in the epoch. Large neural networks take a considerable amount of time for the training and the choice of the learning rate substantially affects this process. Using cyclical learning rates technique helps in the selection of a greater value for

learning rate while still maintaining the improvement of the model. Based on the data distribution, after using the learning rate finder method, we set the learning rate for each experiment individually. We use a weight decay of  $1e-3$  and categorical cross-entropy (equation 5) as the cost function for all the tasks. In equation 5,  $x, y$  denote the classes & observations respectively,  $t_{x,y}$  represent targets and  $p_{x,y}$  represent the predictions. We have limited the training to 10 epochs for our experiments.

$$L_x = - \sum_y t_{x,y} \log(p_{x,y}) \quad (5)$$

The growth rate  $k$  in the DenseNet is the number of output feature maps of a layer, plays an important role in propagating the information through the network. We tried different versions of the DenseNet architecture and the best performance for our task was shown by the DenseNet-161 version. Hereafter, we focus on fine-tuning the selected version. The number 161 refers to the total number of layers in the particular version of the architecture. This can be described as follows: DenseNet-161 consists of 4 dense blocks and hence 3 transition layers between the blocks. There is one convolution layer at the beginning and one classification layer (fully connected layer) at the end. The four dense blocks consist of 12, 24, 72, 48 ‘conv’ layers respectively where ‘conv’ layer is combined BatchNorm, ReLU activation and Convolution. Table 5 describes the functions and the classification head at the end for the model. While the total number of parameters in DenseNet-161 is 28,745,412 freezing initial layers and training only the last layer reduces the number of trainable parameters to 2,493,348.

Initially, we train the last layer for 1-2 epochs. The intuition behind training this way is to train only the fully connected layers completely and freezing the other layers for faster training. This

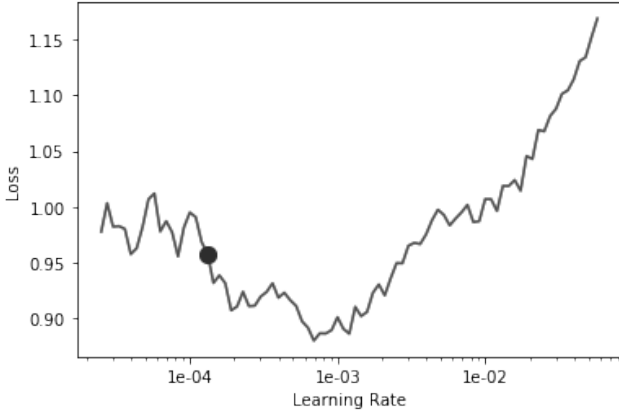


**Figure 5.** Graph of learning rate finder to get optimal learning rate for DenseNet-161 version 1, the black point in the graph depicts the learning rate suggested by the `lr_find` method.

way, we use the weights obtained from the pre-trained model and check the performance of the model. Gradually unfreezing the layers works better than unfreezing and retraining all layers of the network (Yosinski et al. 2014; Howard & Ruder 2018b). Here, we use a set of learning rates instead of a single value to train the network. This technique known as discriminative learning (Howard & Ruder 2018a), is used to obtain the best outcome out of different layers which might need different hyperparameters as per the feature maps in the specific layer. Discriminative learning uses the idea to train the earlier layers with a very low learning rate and the later layers with higher learning rates. This helps to avoid altering the earlier weights and massively affect the end layer weights which are more crucial for the specific case. To update the weights in the network, we require an optimizer and here we use the method of AdamW (Loshchilov & Hutter 2019) to achieve super-convergence (Smith & Topin 2017) which leads to fast training over the data sample even with large architectures such as the one used for our experiments - DenseNet. With the use of a small scale dataset, the model is prone to overfitting as the decision boundaries are based on a few specific samples, here using an efficient regularization technique helps to avoid the overfitting of the model.

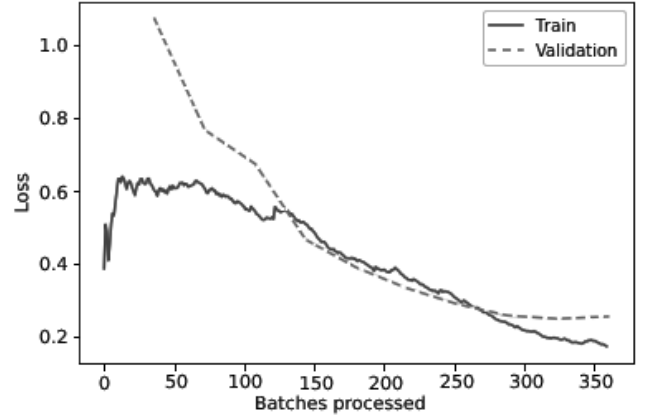
### 3 EXPERIMENTS AND RESULTS

#### 3.1 Version 1: Original set

From Figure 5, we observe that the learning rate between the range  $1e-4$  to  $1e-3$  follows a non-increasing curve and can be used for optimal performance. Using this learning rate and a weight decay of  $1e-3$  we trained Densenet-161 for 10 epochs. The model required 1 minute 10 seconds per epoch leading to a total time of approximately 12 minutes for training.

The training loss starts with a value of 0.6056 (Figure 6) and later follows a downward path with the increase in the number of batches processed. The validation loss starts with a value above 1 (1.07) and later decreases steadily. Near the end of the batch processing, the training and the validation loss reach a value of 0.17 and 0.25 respectively.

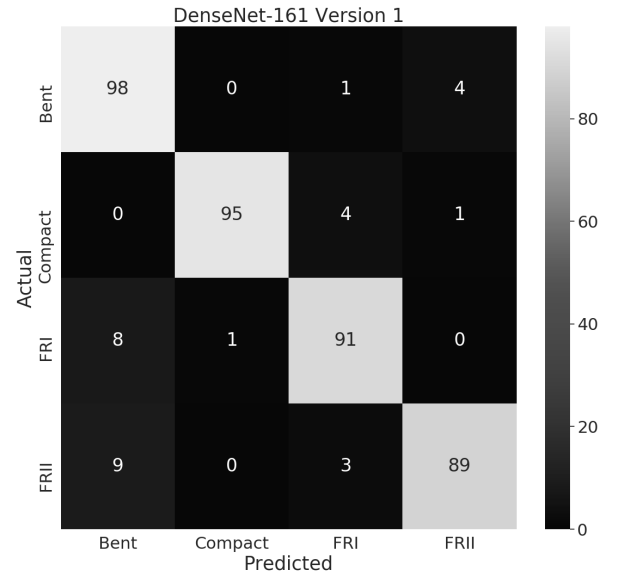
This model performed well on the validation set and the top losses can be observed in some common cases where FR II in predicted as Bent in Figure 8. Individual class metrics for validation set can be observed from Table 6.



**Figure 6.** Plot of training and validation losses as a function of batches processed, DenseNet-161 version 1.

**Table 6.** Validation metrics: DenseNet-161 version 1.

Class	Precision	Recall	F1-Score	Support
Bent	81.57%	93%	86.91%	100
Compact	100%	100%	100%	80
FRI	95.08%	78.37%	85.92%	74
FR II	92.25%	91.61%	91.93%	143
Mean over all classes	92.22%	90.74%	91.19%	397

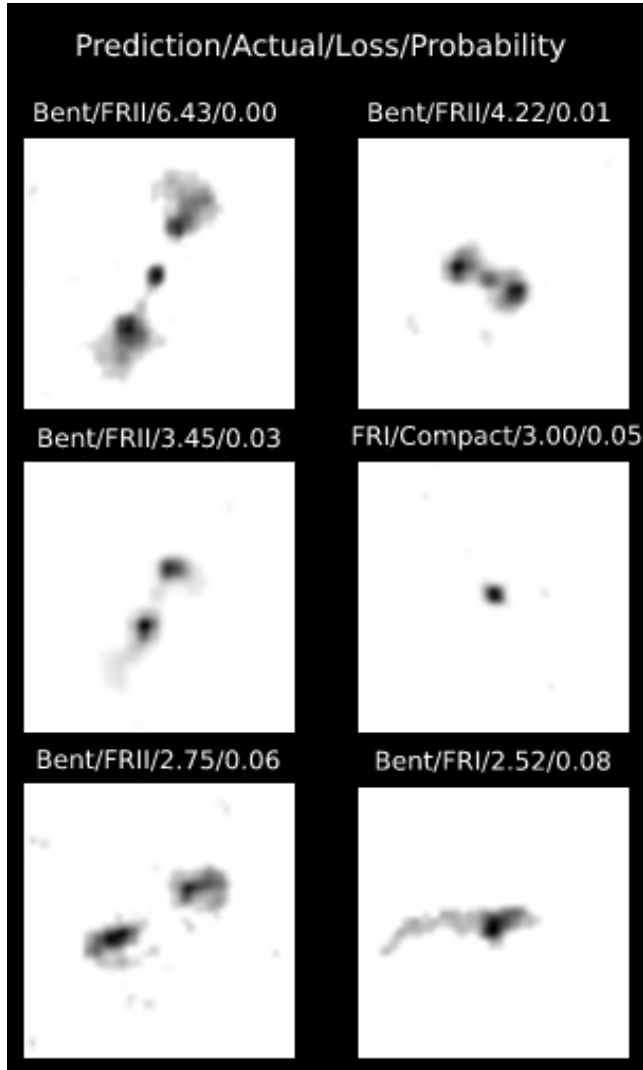


**Figure 7.** DenseNet-161 version 1: test data confusion matrix.

The performance of the model on the test set provided an overall accuracy of 92.3%. The accuracy values per class can be observed from the Figure 7. Individual class metrics for test set can be observed from Table 7.

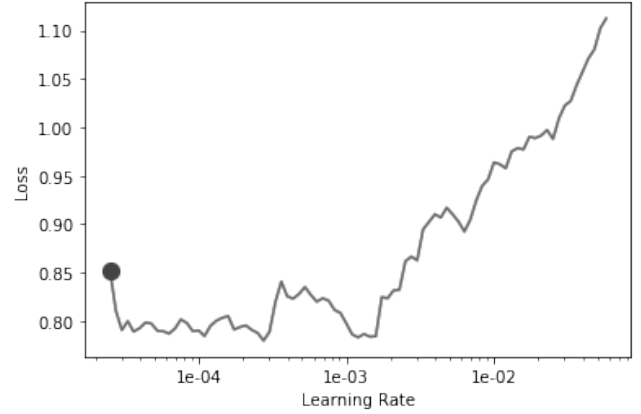
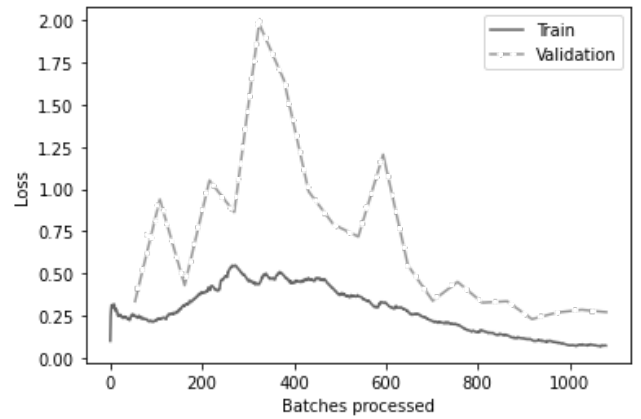
**Table 7.** Test metrics: DenseNet-161 Version 1.

Class	Precision	Recall	F1-Score	Support
Bent	85.21%	95.14%	89.90%	101
Compact	98.95%	95%	96.93%	100
FRI	91.92%	91%	91.46%	100
FRII	94.68%	88.12%	91.28%	103
Mean over all classes	92.69%	92.31%	92.39%	404

**Figure 8.** The top losses and incorrect classification by DenseNet-161 Version 1.

### 3.2 Version 2: balanced dataset

In order to improve the performance, we tried with the balanced data sample (details in section 2.1). Based on the learning rate finder method, here, the learning rate between the range  $3e - 5$  to  $2e - 4$  (Figure 9) follows a decreasing curve and can be used for optimal performance. Using this learning rate and a weight decay of  $1e - 3$  we trained the Densenet-161 pre-trained model with the upsampled classes in the dataset for 10 epochs. The model took a time of 1 minute 38 seconds per epoch leading to a total time of approximately 16 minutes for training.

**Figure 9.** Graph of learning rate finder to get optimal learning rate for DenseNet-161 Version 2.**Figure 10.** Plot of training and validation losses as a function of batches processed, DenseNet-161 Version 2.**Table 8.** Validation metrics: DenseNet-161 Version 2.

Class	Precision	Recall	F1-Score	Support
Bent	84.90%	93.75%	89.10%	144
Compact	98.61%	98.61%	98.61%	144
FRI	93.23%	86.11%	89.53%	144
FRII	92.14%	89.58%	90.84%	144
Mean over all classes	92.22%	92.01%	92.02%	576

The training loss starts with a value of 0.5416 (Figure 10) and later follows a steadily downward path with the increase in the number of batches processed. It reaches a minimum of 0.1588 at the end of the last epoch. The validation loss starts with a value of 0.5116, reaches a minimum value of 0.2598 near the end of the batch processing.

This model performed very well on the validation set with slightly better performance than Version 1 of the DenseNet-161 experiment. The few cases where the sources are classified incorrectly are shown in Figure 11.

The performance of the model on the test set provided an overall accuracy of 92.82%. The accuracy values per class can be observed from the Figure 12. Individual class metrics for test set can be observed from Table 9.



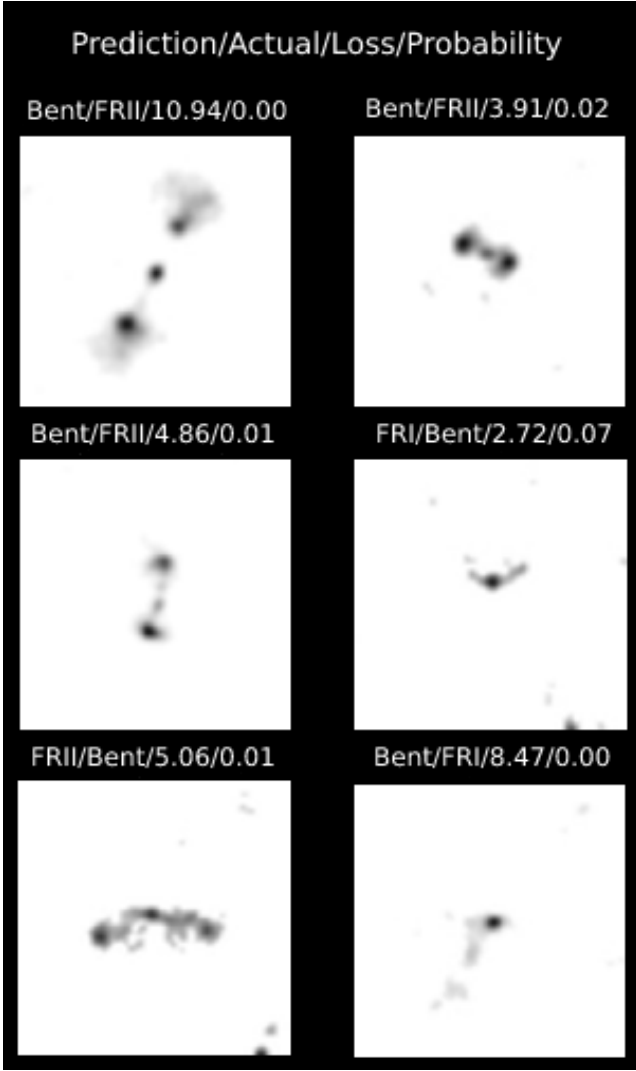


**Figure 11.** The top losses and incorrect classification by DenseNet-161 Version 2.

**Table 9.** Test metrics: DenseNet-161 Version 2.

Class	Precision	Recall	F1-Score	Support
Bent	87.5%	88.35%	87.93%	101
Compact	99%	99%	99%	100
FRI	93%	93%	93%	100
FRII	92%	91.09%	91.54%	103
Mean over all classes	92.87%	92.86%	92.87%	404

#### 4 DISCUSSION AND CONCLUSION

The important part of our work has been the focus on getting accurate classification with few training examples. This factor mainly depends on the task and its complexity. Naturally, a model learns to generalize better with a wide variety of examples rather than just a large number of examples. Deep learning algorithms generate the features from the input data at runtime (training process) and thus avoids the need for feature engineering. To generate useful features, these algorithms require a large amount of data compared to traditional machine learning algorithms. The general idea is to manage

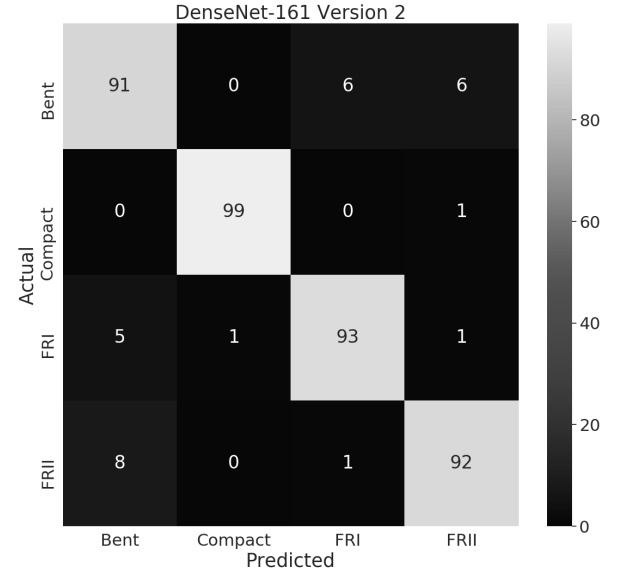


**Figure 12.** DenseNet-161 version 2 (balanced dataset): test data confusion matrix.

the sample size and architecture coherently. In our task, since the number of classes is very less, the number of different parameters per class has not been too high, and thus even with less than 1000 images per class, we have achieved accuracy above 92%. The use of techniques like cyclical learning rate, AdamW optimizer to cope with the less amount of data have helped us to obtain good results with short training time. Though DenseNet has a large number of parameters (section 2.3.2), our training methods help to converge the model quickly, leading to a low cost of training.

In comparison to previous methods, our method outperforms some of these while showing significantly close performance to the other methods. The classification task closely resembles with the work by Alhassan et al. (2018) (similar 4 classes - FRI, FRII, Bent, Compact for classification) in which the authors achieved an overall accuracy above 94% while using more than 21000 samples with 400 epochs for training. In this work, we obtain a close performance with just over 2708 samples in total and 10 epochs for training. Aniyar & Thorat (2017) obtained average precision and recall values of 88% and 86% respectively in their 3 class (FRI, FRII and Bent) classification task using above 25000 samples with augmentation, whereas our classifier obtains average precision of 93.11% and recall of 92.82% for the 4 class classification. Ma et al. (2019) achieved values of 92% and 84% for precision and recall respectively for the 6 class classification task in their two-step approach. Our classifier provides better values for overall precision and recall. Lukic et al. (2018) performed 4 class (Compact, Single extended, Two-Component extended and Multi-component extended) classification and obtained an overall accuracy of 94.8% while using a total of 141032 samples via augmentation (21933 original samples) for 4 classes. Wu et al. (2019) used object detection and classification techniques and obtained mean average precision (mAP) of 84% while using more than 10000 samples. Tang et al. (2019) implemented transfer learning approach while maintaining the idea of domain transfer in their binary classification task (FRI and FRII) and even with the domain transfer approach, authors achieved over-

all accuracy of 90.1% and 83.9% for FIRST and NVSS samples respectively. Lukic et al. (2019) performed a 3 class (Unresolved, FRI and FRII) classification using a model pre-trained on ImageNet dataset and 15936 image samples in total to obtain overall precision of 94.4%.

Few shot learning methods are being developed specifically to make the models efficient in terms of data usage while providing similar results to experiments with larger datasets. In our case, Siamese networks did not perform well but the results are promising. With new techniques being developed in the domain of FSL, better performance can be expected.

Our experiments are driven by the idea to get the best possible performance with as little data as possible. The classifier presented here does not outperform all the previous attempts but we obtain comparable performance with limited data. Convolutional Neural Networks have traditionally worked well with large amounts of data but the recent developments in the training methods have helped to get significant outcome even with fewer samples in the dataset.

The concatenation technique for feature maps in DenseNet helps to capture diverse characteristics rapidly and thus the architecture works well with less amount of data. This has been the primary motivation to utilize DenseNet in our experiments.

Since we are using a network that has already seen a lot of images and learned to distinguish between the classes, we can teach this network to classify the new classes with few examples. The technique has been applied mostly in the same domain tasks but the use of optimal architecture and discriminative learning has helped to obtain better results in a different domain here. Wu et al. (2019) have mentioned regarding the possible negative impact of transfer learning when applied for different domain transfer based on the suggestions from Pan & Yang (2009). Rosenstein et al. (2005) suggested using an ensemble of tasks A for a better transfer to task B mainly due to strong feature space creation. The idea of negative transfer does not practically hold true as seen from our experiments.

The use of data augmentation technique provided only a marginal improvement in our experiments but here we use augmentation only to remove the class imbalance and not extensively to increase the data sample size as performed by previous classifiers.

In both the methods applied in our approach, we observed that the ‘Bent’ category has shown the highest confusion. In the incorrect cases, the FRII samples are classified as Bent and vice-versa. As suggested by Aniyani & Thorat (2017) this is most likely because many Bent galaxies exhibit FRII like appearance and hence can be classified incorrectly as such.

The learning rate finder method based on cyclical learning has provided a way to adapt to the optimal learning rate parameter for all the experiments. The general idea to set the batch size has an aspect of the computational architecture linked to it and thus we set the batch size as a power of 2 i.e. 32, 64 and so on. Larger batch size ( $> 64$ ) can lead to memory overflow but it depends on the network architecture and the data sample. We have maintained a batch size of 32 throughout the experiments. In practice, the batch size and the number of epochs are handled interdependently. The batch size of 32 along with 10 epochs instead of a batch size of 64 and less number of epochs worked better in our experiments. Another important factor, the image size is set as  $224 \times 224$  for our experiments based on the applications of the DenseNet architecture for ImageNet dataset. In order to utilize the weights of the DenseNet obtained for ImageNet dataset, using the ImageNet stats for our data is highly encouraged. The optimizer used in our experiments - AdamW is the improvement over the original Adam (Kingma & Ba 2014) optimizer and performs better for computer vision tasks. The

hyperparameter setup worked best for our case as per the hardware and GPU support but it can be adjusted for different and possibly better results.

Our system can be very useful to classify the objects of any current or future survey. The dataset, experiments and the models are available at [https://github.com/kiryeo/RG\\_Classification\\_code](https://github.com/kiryeo/RG_Classification_code). Users of the system can try to get their own small and curated dataset for the training, tweak with the hyperparameters mentioned above get their own results. Since we are providing the trained model for the inference, users can try using the model as a pre-trained model, perform hyperparameter tuning and get improved results, which is consistent with the domain transfer idea from transfer learning. With the ongoing research for the optimization of neural network architectures, applying the techniques presented in the paper with another architecture can lead to independent results with the same training data.

This paper has been typeset from a  $\text{\TeX}/\text{\LaTeX}$  file prepared by the author.

## REFERENCES

- Alhassan W., Taylor A. R., Vaccari M., 2018, *MNRAS*, **480**, 2085
- Aniyani A. K., Thorat K., 2017, *ApJS*, **230**, 20
- Baldi R. D., Capetti A., Massaro F., 2018, *A&A*, **609**, A1
- Banfield J. K., et al., 2015, *MNRAS*, **453**, 2326
- Becker R. H., White R. L., Helfand D. J., 1995, *ApJ*, **450**, 559
- Blanton E. L., Gregg M. D., Helfand D. J., Becker R. H., White R. L., 2000, *ApJ*, **531**, 118
- Blanton E. L., Gregg M. D., Helfand D. J., Becker R. H., White R. L., 2003, *AJ*, **125**, 1635
- Blum A., Mitchell T., 1998, in COLT’98: Proceedings of the eleventh annual conference on Computational learning theory. pp 92–100
- Bock D. C. J., Large M. I., Sadler E. M., 1999, *AJ*, **117**, 1578
- Burns J. O., 1990, *AJ*, **99**, 14
- Burns J. O., Ledlow M. J., Loken C., Klypin A., Voges W., Bryan G. L., Norman M. L., White R. A., 1996, *ApJ*, **467**, L49
- Capetti A., Massaro F., Baldi R. D., 2017a, *A&A*, **598**, A49
- Capetti A., Massaro F., Baldi R. D., 2017b, *A&A*, **601**, A81
- Carilli C. L., Furlanetto S., Briggs F., Jarvis M., Rawlings S., Falcke H., 2004, *New Astron. Rev.*, **48**, 1029
- Cheng T.-Y., et al., 2020, *MNRAS*, **493**, 4209
- Condon J. J., Cotton W. D., Greisen E. W., Yin Q. F., Perley R. A., Taylor G. B., Broderick J. J., 1998, *AJ*, **115**, 1693
- Dehghan S., Johnston-Hollitt M., Franzen T. M. O., Norris R. P., Miller N. A., 2014, *AJ*, **148**, 75
- Deng J., Dong W., Socher R., Li L.-J., Li K., Fei-Fei L., 2009, in 2009 IEEE conference on computer vision and pattern recognition. pp 248–255
- Dieleman S., Willett K. W., Dambre J., 2015, *MNRAS*, **450**, 1441
- Fanaroff B. L., Riley J. M., 1974, *MNRAS*, **167**, 31P
- Fluke C. J., Jacobs C., 2020, *WIREs Data Mining and Knowledge Discovery*, **10**, e1349
- Gendre M. A., Wall J. V., 2008, *MNRAS*, **390**, 819
- Gendre M. A., Best P. N., Wall J. V., 2010, *MNRAS*, **404**, 1719
- Hadsell R., Chopra S., LeCun Y., 2006, in Proceedings of the 2006 IEEE Computer Society Conference on Computer Vision and Pattern Recognition - Volume 2. CVPR ’06. IEEE Computer Society, Washington, DC, USA, pp 1735–1742, doi:10.1109/CVPR.2006.100, <https://doi.org/10.1109/CVPR.2006.100>
- He K., Zhang X., Ren S., Sun J., 2016, in Proceedings of the IEEE conference on computer vision and pattern recognition. pp 770–778
- Hebb D. O., 1949, The organization of behavior: A neuropsychological theory. Wiley, New York
- Hinton G. E., Osindero S., Teh Y. W., 2006, *Neural Computation*, **18**, 1527
- Hocking A., Geach J. E., Sun Y., Davey N., 2018, *MNRAS*, **473**, 1108

- Howard J., Ruder S., 2018a, in ACL. Association for Computational Linguistics, <http://arxiv.org/abs/1801.06146>
- Howard J., Ruder S., 2018b, CoRR, abs/1801.06146
- Howard J., et al., 2018, fastai, <https://github.com/fastai/fastai>
- Huang G., Liu Z., Van Der Maaten L., Weinberger K. Q., 2017, in Proceedings of the IEEE conference on computer vision and pattern recognition. pp 4700–4708
- Huertas-Company M., et al., 2015, *ApJS*, **221**, 8
- Ioffe S., Szegedy C., 2015a, in Bach F., Blei D., eds, Proceedings of Machine Learning Research Vol. 37, Proceedings of the 32nd International Conference on Machine Learning. PMLR, Lille, France, pp 448–456, <http://proceedings.mlr.press/v37/ioffe15.html>
- Ioffe S., Szegedy C., 2015b, CoRR, abs/1502.03167
- Johnston S., et al., 2008, *Experimental Astronomy*, **22**, 151
- Jonas J., MeerKAT Team 2016, in MeerKAT Science: On the Pathway to the SKA. p. 1
- Kingma D. P., Ba J., 2014, Adam: A Method for Stochastic Optimization, <http://arxiv.org/abs/1412.6980>
- Koch G., 2015.
- Kolesnikov A., Beyer L., Zhai X., Puigcerver J., Yung J., Gelly S., Houlsby N., 2019, arXiv e-prints, [p. arXiv:1912.11370](https://arxiv.org/abs/1912.11370)
- Krizhevsky A., Sutskever I., Hinton G. E., 2012, in Pereira F., Burges C. J. C., Bottou L., Weinberger K. Q., eds, , Advances in Neural Information Processing Systems 25. Curran Associates, Inc., pp 1097–1105, <http://papers.nips.cc/paper/4824-imagenet-classification-with-deep-convolutional-neural-networks.pdf>
- Lake B. M., Salakhutdinov R., Gross J., Tenenbaum J. B., 2011, One shot learning of simple visual concepts
- LeCun Y., Cortes C., Burges C., 2010, ATT Labs [Online]. Available: <http://yann.lecun.com/exdb/mnist>, 2
- LeCun Y., Bengio Y., Hinton G., 2015, *Nature*, **521**, 436
- Loshchilov I., Hutter F., 2019, in International Conference on Learning Representations. <https://openreview.net/forum?id=Bkg6RiCqY7>
- Lukic V., Brüggen M., Banfield J. K., Wong O. I., Rudnick L., Norris R. P., Simmons B., 2018, *MNRAS*, **476**, 246
- Lukic V., Brüggen M., Mingo B., Croston J. H., Kasieczka G., Best P. N., 2019, *Monthly Notices of the Royal Astronomical Society*, **487**, 1729
- Luo C., Li X., Wang L., He J., Li D., Zhou J., 2018, in 2018 5th International Conference on Systems and Informatics (ICSAI). pp 361–366
- Ma Z., et al., 2019, *ApJS*, **240**, 34
- Mao M. Y., Johnston-Hollitt M., Stevens J. B., Wotherspoon S. J., 2009, *MNRAS*, **392**, 1070
- Mao M. Y., Sharp R., Saikia D. J., Norris R. P., Johnston-Hollitt M., Middelberg E., Lovell J. E. J., 2010, *MNRAS*, **406**, 2578
- Martin G., Kaviraj S., Hocking A., Read S. C., Geach J. E., 2020, *MNRAS*, **491**, 1408
- McCulloch W., Pitts W., 1943, *Bulletin of Mathematical Biophysics*, **5**, 127
- Miley G. K., Perola G. C., van der Kruit P. C., van der Laan H., 1972, *Nature*, **237**, 269
- Nair V., Hinton G. E., 2010, in Proceedings of the 27th international conference on machine learning (ICML-10). pp 807–814
- Norris R. P., et al., 2011, *Publ. Astron. Soc. Australia*, **28**, 215
- Ostrovski F., et al., 2017, *MNRAS*, **465**, 4325
- Pan S. J., Yang Q., 2009, *IEEE Transactions on knowledge and data engineering*, **22**, 1345
- Paszke A., et al., 2019, in Advances in neural information processing systems. pp 8026–8037
- Philip N. S., Wadadekar Y., Kembhavi A., Joseph K. B., 2002, *A&A*, **385**, 1119
- Pratt L. Y., 1993, in Advances in neural information processing systems. pp 204–211
- Proctor R. N., de Oliveira C. M., Dupke R., de Oliveira R. L., Cypriano E. S., Miller E. D., Rykoff E., 2011, *MNRAS*, **418**, 2054
- Roettiger K., Burns J. O., Loken C., 1996, *ApJ*, **473**, 651
- Roh Y., Heo G., Whang S. E., 2018, A Survey on Data Collection for Machine Learning: a Big Data – AI Integration Perspective ([arXiv:1811.03402](https://arxiv.org/abs/1811.03402))
- Rosenblatt F., 1958, *Psychological Review*, **65**, 386
- Rosenstein M., Marx Z., Dietterich T. G., Kaelbling L. P., 2005, in NIPS 2005.
- Rudnick L., Owen F. N., 1976, *ApJ*, **203**, L107
- Rumelhart D. E., Hinton G. E., Williams R. J., 1986, *Nature*, **323**, 533
- Schawinski K., Zhang C., Zhang H., Fowler L., Santhanam G. K., 2017, *MNRAS*, **467**, L110
- Smith L. N., 2015, arXiv e-prints, [p. arXiv:1506.01186](https://arxiv.org/abs/1506.01186)
- Smith L. N., Topin N., 2017, arXiv e-prints, [p. arXiv:1708.07120](https://arxiv.org/abs/1708.07120)
- Soekhoe D., van der Putten P., Plaat A., 2016, in Boström H., Knobbe A., Soares C., Papapetrou P., eds, Advances in Intelligent Data Analysis XV. Springer International Publishing, Cham, pp 50–60
- Tan C., Sun F., Kong T., Zhang W., Yang C., Liu C., 2018, arXiv e-prints, [p. arXiv:1808.01974](https://arxiv.org/abs/1808.01974)
- Tang H., Scaife A. M. M., Leahy J. P., 2019, *MNRAS*, **488**, 3358
- Wang H., Raj B., Xing E. P., 2017, CoRR, abs/1702.07800
- Wing J. D., Blanton E. L., 2011, *AJ*, **141**, 88
- Wu C., et al., 2019, *MNRAS*, **482**, 1211
- Yalniz I. Z., Jégou H., Chen K., Paluri M., Mahajan D., 2019, CoRR, abs/1905.00546
- Yosinski J., Clune J., Bengio Y., Lipson H., 2014, in Advances in neural information processing systems. pp 3320–3328